The University of Washington Shallow Convection and Moist Turbulence Schemes and Their Impact on Climate Simulations with the Community Atmosphere Model

SUNGSU PARK AND CHRISTOPHER S. BRETHERTON

Department of Atmospheric Sciences, University of Washington, Seattle, Washington

(Manuscript received 2 April 2008, in final form 5 December 2008)

ABSTRACT

This paper describes a new version of the University of Washington shallow cumulus parameterization. The new version includes improved treatments of lateral mixing rates into cumulus updrafts, the evaporation of precipitation and of the interaction of cumuli with the underlying subcloud layer, and a treatment of the convective inhibition-based mass-flux closure that is more numerically stable and is suitable for the long time steps of global climate models.

The paper also documents its performance when combined with a new moist turbulence parameterization in simulations with version 3.5 of the Community Atmosphere Model (CAM3.5). A single-column simulation of nonprecipitating trade cumulus shows considerable improvements in vertical thermodynamic structure and less resolution sensitivity in the new schemes compared to CAM3.5. In global simulations, the new schemes, combined with an increase of vertical resolution from 26 to 30 levels, produce a significant (7%) reduction in overall climate bias, calculated from root-mean-squared error of the seasonal model climatology compared to a suite of global observations of various fields. Biases in almost all fields, particularly the shortwave cloud radiative forcing, are reduced. Geographical bias patterns in surface rainfall, liquid water path, and surface air temperature are only mildly affected by the model parameterization and vertical resolution changes.

1. Introduction

Cloud-topped planetary boundary layers (PBLs) modulate surface turbulent and radiative fluxes over most of the globe. They play a key role in the earth's current radiation balance, climate sensitivity, and aerosol indirect effects on climate. Physically realistic parameterizations of the turbulent and cloud microphysical processes that maintain cloud-topped PBLs are therefore a central requirement for modern climate simulation models. Both "layer" turbulence (as in a stratocumulus-capped mixed layer or the subcloud layer underneath shallow cumulus convection) and cumulus convection must be represented. They must interact appropriately with each other and with other moist physical parameterizations.

This paper describes the performance of new moist turbulence and shallow cumulus parameterizations developed at the University of Washington (UW) in global climate simulations with version 3.5 of the Community Atmosphere Model (CAM3.5), a major atmospheric general circulation model (AGCM). These schemes are replacements for the Holtslag and Boville (1993) PBL scheme, a simple downgradient turbulent mixing scheme in the free troposphere, and the Hack (1994) shallow cumulus parameterization currently used in CAM3.5. In the last few years, other AGCMs have also modernized their treatments of stratocumulus-capped PBL dynamics or shallow cumuli (e.g., Lock et al. 2000; von Salzen and McFarlane 2002; GAMDT 2004). Our parameterizations have some novel characteristics, our implementation involved several noteworthy related changes to other moist physics parameterizations in CAM, and CAM is a widely used model. This makes it worthwhile to document our new parameterizations and their effect on the simulated CAM3.5 climate. Since the UW moist turbulence and shallow convection tightly interact and have been designed to work with each other, we focus on documenting their combined performance.

Unlike the current CAM3.5 turbulence schemes, which assume no direct interaction between turbulence

Corresponding author address: Christopher S. Bretherton, Department of Atmospheric Sciences, Box 351640, University of Washington, Seattle, WA 98195-1640.
E-mail: breth@atmos.washington.edu

DOI: 10.1175/2008JCLI2557.1

and condensation, the UW moist turbulence (UWMT) parameterization is formulated using moist thermodynamics. It treats surface-based and elevated turbulent layers in a unified framework. It is a downgradient mixing scheme with an explicit entrainment parameterization at the edge of layers of convective turbulence, and a novel diagnosis of turbulent kinetic energy (TKE) used to determine the eddy diffusivity in turbulent layers. The Holtslag–Boville scheme assumes that surface fluxes are the only energy source for the turbulence; in UWMT, turbulence is affected by all processes that affect the vertical structure of the atmosphere, notably radiative cooling.

In a companion paper (Bretherton and Park 2009, hereafter BP09), we describe the UWMT scheme as implemented in CAM3.5. BP09 use single-column modeling tests to compare its performance with the current turbulent mixing schemes. We find that the new scheme gave comparable or better results to the current CAM3.5 for dry convective and stable PBLs. For a nocturnal stratocumulus-capped PBL, the Hack shallow cumulus scheme is active at operational vertical resolution and dominates entrainment process, leading to stratocumulus whose thickness is highly sensitive to vertical resolution. The UWMT scheme produces more realistic and less resolution-sensitive results for this case. The Hack scheme mixes triplets of model layers when conditional instability is diagnosed, with adjustable efficiencies for penetrative entrainment and precipitation. As illustrated in BP09, it acts in CAM as a moist-adjustment scheme for conditionally unstable layer clouds as well as for cumulus convection. It is resolution sensitive because it is not derived from a continuous differential equation and does not have a consistent limit as the vertical grid spacing is refined.

The UW shallow cumulus (UWShCu) parameterization derives from Bretherton et al. (2004a, hereafter BMG04), who implemented it for regional climate simulations of subtropical stratocumulus to trade cumulus transitions in the northeast and southeast Pacific using a mesoscale model. UWShCu is a mass-flux scheme in which entrainment and detrainment into a bulk cumulus updraft are derived using a buoyancy-sorting algorithm, similar to Kain and Fritsch (1990). It has a combined mass-flux closure and trigger based on convective inhibition (CIN). It has undergone extensive single-column model testing; one example will be shown in this paper. Its CAM implementation has undergone extensive refinement, as documented in this paper.

Our paper is organized as follows. In section 2, we summarize the UWShCu scheme, focusing on new features in the CAM implementation. We also review highlights of the UW moist turbulence scheme relevant to understanding our GCM simulation results. Section 3 describes other changes made to CAM3.5 for use with the UW schemes; the resulting model configuration will be hereafter called CAMUW. Section 4 discusses a single-column application to a nonprecipitating shallow cumulus case. In section 5, we compare the climate simulation skill of CAMUW and CAM3.5 using a small set of global metrics that can be combined into a single climate bias index. Section 6 compares the global climatologies of CAMUW and CAM3.5 simulations in more detail, focusing on cloud-related variables. Section 7 discusses the simulated vertical boundary layer structure in the southeast and northeast Pacific subtropical stratocumulus regimes. Section 8 presents a summary and conclusions.

2. Implementation of the UW shallow cumulus scheme in CAM

The UW moist turbulence scheme as implemented in CAM3.5 is described in BP09. Here we describe the UW shallow cumulus scheme, noting changes from the earlier version of BMG04.

Figure 1 shows how the UW shallow convection scheme operates in a typical trade cumulus regime. Vertical convective fluxes of two moist adiabatically conserved variables, the total specific humidity $q_t = q_v + q_c$ and the liquid water potential temperature θ_l, and of the horizontal velocity components u and v are computed at interfaces between layers. We label bulk cumulus updraft properties with the subscript u, and horizontal averages across a grid cell with an overbar. The cumulus flux of an arbitrary quantity a is represented as the product of a cumulus updraft mass flux M_u and the updraft-environment difference of a. Downdraft fluxes are not explicitly included, since they are less important for shallow cumulus convection than for deep convection. Assuming that the area fraction of the convective updraft is negligibly small,

$$\overline{w'a'} = \frac{M_u}{\rho}(a_u - \bar{a}), \tag{1}$$

where w is vertical velocity and ρ is air density.

Following BMG04, the bulk cumulus updraft is modeled as a buoyancy-sorting entraining–detraining plume rising from the PBL top. Given profiles of fractional lateral entrainment rate $\varepsilon(z)$ and detrainment rate $\delta(z)$, standard updraft dilution equations [Eqs. (13) and (14) of BMG04] determine the vertical evolution of mass flux and transported quantities. The equations for u_u and v_u include a correction for horizontal pressure gradient acceleration following Gregory et al. (1997). We also diagnose a profile of bulk updraft vertical velocity w_u,

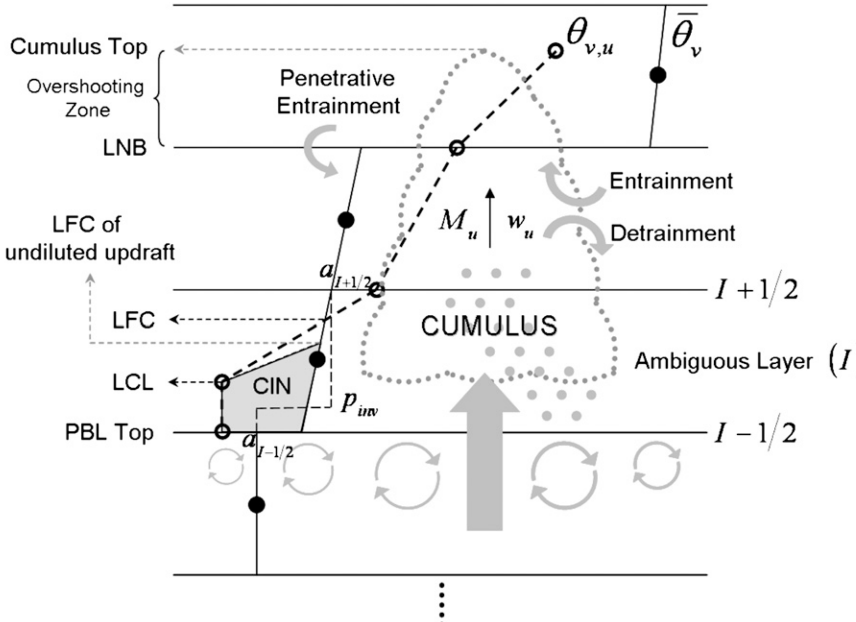

FIG. 1. Schematic structure of UW shallow cumulus scheme describing vertical evolution of a bulk cumulus updraft and its interaction with the environment and the subcloud layer. Black dots denote grid-layer mean virtual potential temperature $\bar{\theta}_v$, from which a θ_v profile (solid line) is reconstructed. The horizontal solid lines are flux interfaces, where the updraft virtual potential temperature $\theta_{v,u}$ (open circles) is computed, from which a cumulus updraft θ_v profile (dashed) is reconstructed. The "I" indicates the ambiguous layer, and $p_{\rm inv}$ is the reconstructed PBL capping inversion within this layer. Environmental conservative variables reconstructed just above and below the ambiguous layer are denoted by $a_{I+1/2}$ and $a_{I-1/2}$, respectively. See section 2 and the appendix for details.

which determines the plume depth, enters the calculation of entrainment and detrainment rates, and is used together with M_u in calculating the fractional area of shallow cumuli. Currently, the plume microphysics are highly simplified—if the amount of cumulus condensate becomes larger than a threshold $q_{c,\max} = 1$ g kg^{-1}, the excess is precipitated. The partitioning of cumulus updraft condensate and precipitation between liquid and ice phases follows the CAM3 stratiform microphysics scheme (Rasch and Kristjansson 1998). The CAM implementation of the UWShCu scheme discretely conserves energy and moisture.

The specifications of entrainment and detrainment rates (including "penetrative entrainment" above the plume's level of neutral buoyancy), cloud-base properties, and the CIN-based mass-flux closure follow BMG04, except for the following modifications detailed in the appendix:

- For improved numerical stability with long time steps, cumulus mass flux is computed using a CIN estimated implicitly at the end of the time step.
- The treatment of cumulus fluxes within the PBL has been improved.
- The lateral updraft-environment mixing rate and buoyancy-sorting algorithms have been modified to be more consistent with large-eddy simulations (LES) of shallow cumuli.
- The evaporation of precipitation from the cumulus updraft has been revised, also based on LES.

The tunable model parameters in UWShCu are listed in Table 1. For each parameter, the value currently used in CAMUW and a plausible range are given. These choices are discussed further in the final section of the appendix.

While the UWShCu scheme is optimized to represent shallow cumulus convection, it can simulate deep convection as well. We have in fact run CAMUW without the default Zhang and McFarlane (1995) deep convection parameterization and obtained encouraging results for the climatological distribution of rainfall and sea level pressure that in some ways improve on CAM3.5. However, to develop UWShCu into an attractive unified parameterization for shallow and deep cumulus convection would require refined treatments of updraft lateral mixing rates and buoyancy sorting, convective downdrafts, and updraft microphysics that are more

TABLE 1. Tunable parameters and their recommended ranges in the UW shallow cumulus scheme.

Parameter	Description	Value	Possible range
c	Fractional mixing efficiency	8	4–8
r_{pen}	Penetrative entrainment efficiency	10	1–10
$A_{u,\max}$	Maximum core updraft fractional area	0.1	0.05–0.15
$q_{c,\max}$	Maximum updraft condensate	1 g kg^{-1}	0.5–1.5 g kg^{-1}

appropriate for deep convection—these are still topics of ongoing research.

3. Simulation setup

We implemented the UW moist turbulence and shallow convection schemes into the National Center for Atmospheric Research (NCAR) Community Atmospheric Model, version 3 (CAM3). The publicly released version, CAM3.0, is documented in Collins et al. (2006). Over the last years, there have been continuous efforts to upgrade CAM3. The current version CAM3.5 uses 1) a finite-volume (FV) dynamical core suitable for chemical transport modeling instead of a spectral Eulerian core as the default, 2) a new land model, 3) modifications to the cumulus momentum transport (Richter and Rasch 2008) and mass-flux closure of the deep convection scheme (Neale et al. 2008), 4) an artificial reduction of low-level cloud fraction at low specific humidity designed to remove excessive low-level high-latitude winter cloud in CAM3.0, and 5) a slight change to the stratiform condensation scheme that we will describe later. Together, these changes produce a 10%–20% decrease in most global climate biases (as defined in section 5) compared to CAM3.0 (Neale et al. 2008), including improvements in tropical surface winds, El Niño–Southern Oscillation (ENSO), and high-latitude land surface temperatures. We document the effect of the UW schemes on CAM3.5, since it is the current state of the art for CAM.

The performance and biases of the UW schemes are strongly influenced by the other CAM3.5 model physics, especially the stratiform cloud and deep convection schemes. Improving the skill of the whole system involves not only upgrading the component parameterizations, but also ensuring they are interacting as expected. CAM is "process split"—in each time step, successive parameterizations operate on the updated state resulting from the previous parameterization. The physical parameterizations in CAM are called in the following order: deep convection → shallow cumulus → stratiform cloud fraction, condensation, and precipitation → radiation → surface fluxes → turbulence diffusion.

We do not put any restrictions on the depth over which UWShCu can operate. The prior call to the deep cumulus scheme, which triggers easily and aggressively stabilizes the tropospheric column, is sufficient to restrict UWShCu to shallow cumulus regimes. The deep cumulus scheme also plays a central role in determining the simulated temperature profile and large-scale circulation of the tropics and extratropics, inducing biases to which the shallow cumulus and turbulence schemes are slaved.

The interactions among the shallow cumulus, stratiform cloud parameterizations, and radiation schemes are problematic. In the current CAM3.5, the shallow cumulus scheme outputs a cumulus cloud fraction to the radiation scheme, but the condensate within that cumulus cloud must be generated within the stratiform macrophysics scheme. This does not ensure a realistic condensate profile within a shallow cumulus cloud. The condensate at any grid level is affected by detrainment of condensate from the cumulus scheme. It is not obvious how to best specify this, since it is the condensate within the cumuli themselves that we want to reproduce by this "detrainment." In addition, there are cloud overlap issues. LES show that the cumulus cloud fraction in a typical trade cumulus ensemble is typically well under 10% at any level, but the overall column cloud fraction may be 20%–30% because of cloud tilt and life cycle effects. CAM's current radiation scheme assumes maximum random overlap of cloud fraction, which in this case will be a gross underestimate of the true column cloud fraction, even if the cloud fraction at all grid levels is correct.

The turbulence scheme also interacts tightly with other physical parameterizations. While this is physically appropriate, problems can arise because each parameterization sequentially updates the thermodynamic and wind profile. Thus the parameterizations all work on slightly different and hence mutually inconsistent profiles. We note two such issues that we have experienced with CAMUW. First, the surface fluxes are computed before the turbulent scheme, so the surface winds produced by the turbulence scheme may not be consistent with the surface stresses. This can lead to numerical instability with the long time steps used in CAM. Second, in the UW moist turbulence scheme, cloud-top radiative cooling and condensational heating can be very important in driving turbulence and entrainment. The cloud properties are diagnosed from the stratiform macrophysics scheme, which is not working on exactly the same thermodynamic profile as the turbulence scheme. Hence, clouds can sometimes form in unexpected places, such as within the grid layer above a cloud-topped boundary layer. Such interactions can significantly affect the performance of the turbulence scheme.

Other than the turbulence and shallow convection schemes, the main difference between CAM3.5 and CAMUW is that two artificial controls on low-cloud cover in CAM3.5 are not used in CAMUW. These are the marine stratiform low-cloud fraction parameterization in CAM3 (from Klein and Hartmann 1993) and an ad hoc restriction on low-cloud cover in dry conditions ($q_v <$ 3 g kg^{-1}) applied in CAM3.5 to reduce high-latitude wintertime low-cloud cover. CAMUW uses only the relative humidity and convective cloud fraction to deduce the overall cloud fraction.

We ran the CAM3.5 and CAMUW at 1.9° latitude × 2.5° longitude resolution using the FV dynamic core and an 1800-s time step. CAM3.5 was run with 26 vertical grid layers and CAMUW with 30 layers. We added the extra 4 layers in the lower troposphere in order to improve the simulation of turbulent eddy motion within the PBL capped by stratocumulus clouds that are frequently observed to be thinner than the L26 grid-layer thickness. Simulations are forced by seasonally varying climatological sea surface temperature (SST) and sea ice extent for 6 yr, and the last 5 yr of simulations were used for analysis. The land and sea ice models are fully interactive.

The critical relative humidities RH_c for low-level (below 750 hPa) and high-level (above 750 hPa) cloud fraction are used to tune the global annual-average top-of-atmosphere shortwave and longwave radiative energy fluxes in both versions of CAM close to observations. The CAM3.5 simulations use low (high) RH_c of 0.915 (0.80), while CAMUW simulations use low (high) RH_c of 0.93 (0.88).

4. BOMEX single-column results

Before looking at global simulations, it is illuminating to compare CAMUW and CAM3.5 on a benchmark single-column shallow cumulus case, the Global Energy and Water Cycle Experiment (GEWEX) Cloud System Study (GCSS) Barbados Oceanography and Meteorology Experiment (BOMEX) case described by Siebesma et al. (2003). This is a case of shallow nonprecipitating tropical trade cumulus forced based on observations. Simulations are run 6 h from a specified initial sounding with surface fluxes, geostrophic wind, radiative cooling, and subsidence. Results are compared with an identically forced LES run by Peter Blossey using version 6.5 of the System for Atmospheric Modeling (Khairoutdinov and Randall 2003). The LES domain and resolution follow Siebesma et al. (2003), who also found that, for this case, there was very little spread in the cumulus and turbulence statistics between different LES models.

Figure 2 compares LES and single-column output averaged over the final 3 h of simulation, after initial transients have died down. The top two rows of plots show results from CAMUW and CAM3.5 with the 30-layer grid (L30) used in the global CAMUW simulations. In contrast to the global CAM simulations, which use a FV dynamical core, the single-column CAM can only use an Eulerian dynamic core, for which the default time step for global integrations is 1200 s. Hence this time step is also used in the L30 single-column simulations shown here. The bottom row shows results with a much higher-resolution 80-layer grid (L80) and a 300-s time step.

The top row shows profiles of liquid potential temperature, total specific humidity, and the two horizontal velocity components. The CAMUW and LES profiles all agree quite well. The CAM3.5 tends to develop a shallower trade inversion and does not mix momentum as well across the subcloud layer. These results are similar with 80 layers (not shown).

The second row shows the L30 simulated cumulus cloud properties. The cumulus cloud fraction in CAM3.5 is a nonlinear function of cumulus mass flux that overestimates the cloud fraction at each level, though it simulates the column cloud fraction better. Below 500 m, CAM3.5 also predicts significant additional stratiform cloud because of the high relative humidity. The result, seen in Fig. 2e, is that CAM3.5 greatly overestimates the horizontally averaged liquid water content (LWC) at most levels below the trade inversion. The CAM3.5 updraft mass flux (Fig. 2f) has the right magnitude but does not penetrate high enough into the trade inversion. The 80-level CAM3.5 results are quite different, as seen in Figs. 2g–i. At this vertical resolution, the Hack shallow cumulus parameterization turns off altogether, and a deep, thick stratocumulus layer develops in its place. This is an example of how the Hack scheme renders the CAM3.5 very sensitive to vertical resolution.

In contrast, the CAMUW cumulus cloud fraction and updraft mass flux are insensitive to vertical resolution and agree fairly well with LES. The grid-mean LWC computed internally by UWShCu as the product of updraft fraction and updraft LWC (CAMUW-cumulus in Figs. 2e,h) is also in good agreement with LES. However, the cloud LWC that would be seen by the radiation scheme, if it were used in the simulation, is that which comes from the stratiform cloud scheme, shown as "CAMUW" in Figs. 2e,h. Disturbingly, this cloud LWC is zero at all levels except near cloud base at

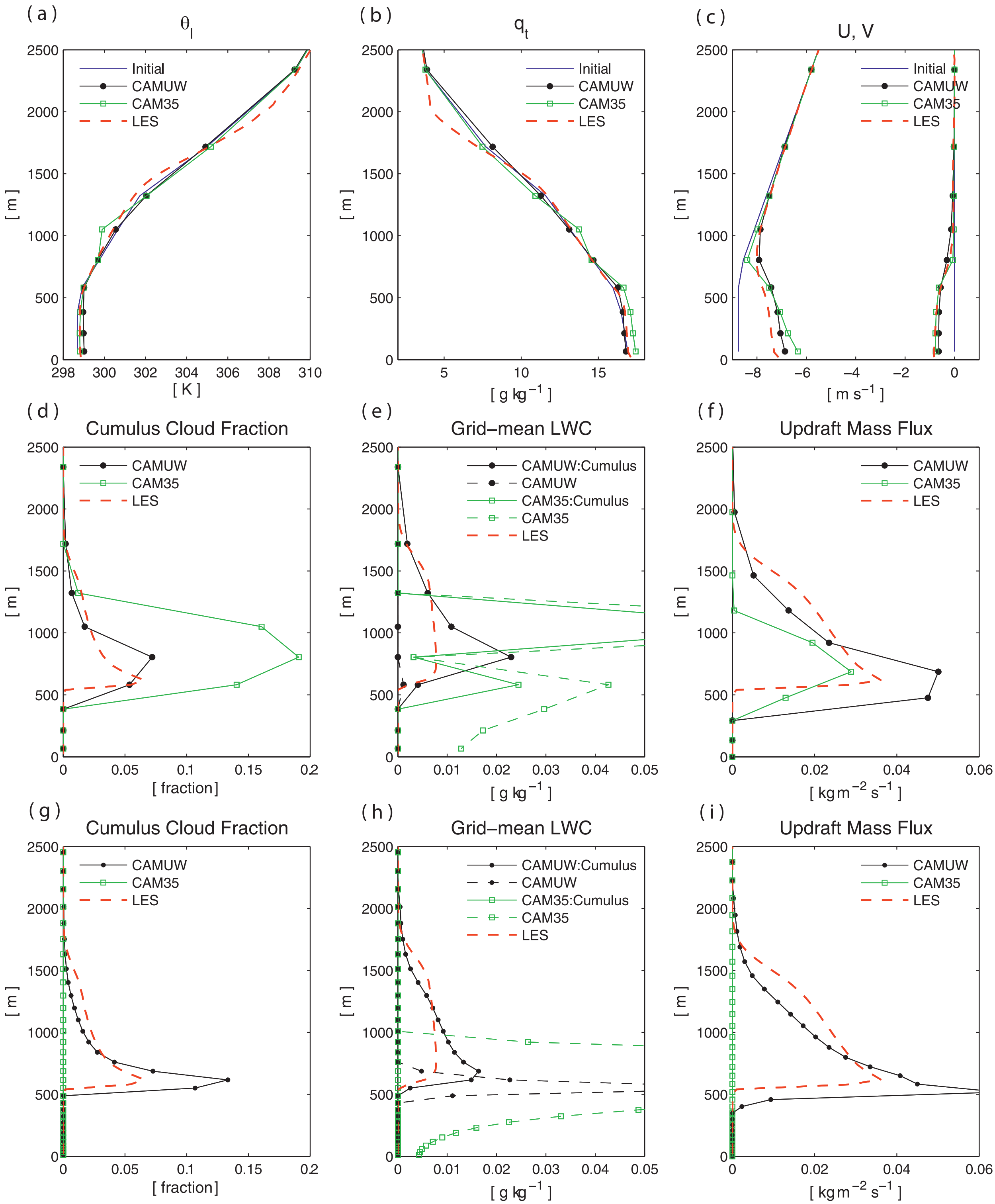

FIG. 2. Single-column comparison of CAM3.5 and CAMUW on BOMEX shallow cumulus case, averaged over the last 3 h of the simulation. (top),(middle) 30-level simulations with Δt = 1200 s; (bottom) 80-level simulation with Δt = 300 s.

L80. This is true even though UWShCu detrains liquid water in a plausible way from the cumulus updrafts. It indicates a poor interaction between UWShCu and the CAM stratiform condensation scheme. The same problem will be evident in the global simulations, where it affects both atmospheric and oceanic radiative cooling, circulation, and climate. We are currently working to find a satisfying solution for this problem. One possible approach is to assign separate subcolumns to cumulus clouds independent of those used for stratiform clouds (i.e., subcolumn approach, Pincus et al. 2003). The fractional area and LWC of cumulus subcolumns can then be directly computed by the cumulus parameterization.

We have also simulated other GCSS single-column shallow cumulus cases using CAMUW, including a continental shallow cumulus case (Brown et al. 2002) and the current precipitating trade cumulus case. While we do not have space to discuss these results here, we have used them in refining the cloud-base mass-flux closure, the representation of precipitation evaporating from cumulus updrafts, and other aspects of UWShCu.

5. Global climatological skill of CAMUW and CAM3.5

A climate model is a complex system of interacting software modules. Changes in one module, even if based on sound physical arguments and backed up by single-column testing, do not necessarily improve the system performance. It is therefore useful to have simple objective measures of the climatological skill of a simulation.

We evaluate the global skill of our simulations using a ''climate bias index'' based on a comprehensive set of 9 metrics that encompass atmospheric circulations and vertical thermodynamic structures, surface precipitation, land surface temperature, and cloud radiative effects over the seasonal cycle. These metrics should be based on reliable observational datasets extending over many annual cycles, and should reflect aspects of the simulation that might affect CAM's performance as part of a climate system model including the ocean, the stratosphere, chemistry, or vegetation changes.

The five purely observational datasets we choose are all part of the CAM's standard diagnostics package, and are all monthly-mean climatologies averaged over the years indicated below. They are surface wind stress over ocean (1992–2000) from the European Remote Sensing (ERS) scatterometer (Bentamy et al. 1996), surface rainfall (1979–2003) from the Global Precipitation Climatology Project (GPCP; Adler et al. 2003), near-surface air temperature over land (1950–99) from Willmott and Matsuura (1995), and top-of-atmosphere (TOA) shortwave and longwave cloud radiative forcings (2000–03) derived from the National Aeronautics and Space Administration's (NASA) Clouds and the Earth's Radiant Energy System (CERES) scanners. While this CERES ''climatology'' only spans 4 yr, we believe it is representative because the two dominant modes strongly influencing interannual variations of global clouds, ENSO and the Arctic Oscillation (Park and Leovy 2004, 2000) were in weakly positive or neutral phases in this period.

We use four other comparison datasets from the 40-yr European Centre for Medium-Range Weather Forecasts (ECMWF) Re-Analysis (ERA-40; Uppala et al. 2005). These are 1980–2001 climatologies of sea level pressure, zonal wind at 300 hPa, and the three-dimensional temperature and relative humidity fields. The metrics we use have also been adopted for model evaluation by Neale et al. (2008), except that they use equatorial wind stress in place of global wind stress and separately score land and ocean precipitation. Gleckler et al. (2008) have also experimented with simple metrics of climate model performance.

For each field, the model climatology is calculated at each grid point and season [December–February (DJF), March–May (MAM), June–August (JJA), and September–November (SON)]. The root-mean-square (rms) error between model and observation over all grid points and seasons is calculated. For the kth field, we denote this rms error by ε_k. We find that a 5-yr simulation is adequate to reliably estimate ε_k to within 1%–2% for the fields we consider. A control model is picked—we choose CAM3.0. For each field, we calculate the ''error ratio'' $\mathrm{ER}_k = \varepsilon_k/\varepsilon_k^{\mathrm{CAM3.0}}$ of the average rms error to that in the control model. We then take the mean of the error ratios for all $N = 9$ fields to get a ''climate bias index'' (CBI):

$$\mathrm{CBI} = N^{-1}\sum_{k=1}^{N}\mathrm{ER}_k. \qquad (2)$$

A lower CBI indicates a simulation with smaller average space–time biases over the seasonal cycle. The CBI depends upon the chosen fields. However, our experience is that the error ratios of different fields are often somewhat correlated, such that improvements in one field tend to go with improvements in other fields. This makes the exact choice of fields less important. The approach could easily be extended to the atmospheric climatology of coupled simulations by adding SST as a comparison field.

Inevitably, each observational dataset contains its own biases, and quantities such as near-surface air temperature

TABLE 2. The error ratio of rmse of the simulation to the rmse of CAM3.0. The rmse of CAM3.0 in physical unit is in the rightmost column. Numbers in bold indicate at least a 5% decrease in the ratio for one model compared to the other.

Variable	Observed data	CAM3.5	CAMUW	CAM3.0 rmse
SLP	ERA-40 1980–2001. Global	0.82	**0.75**	3.5 hPa
Surface wind stress	ERS scatterometer 1992–2000. Ocean	0.82	0.78	0.05 N m^{-2}
Zonal wind at 300 hPa	ERA-40 1980–2001. Global	0.77	**0.68**	4.5 m s^{-1}
Surface rainfall	GPCP 1979–2004. Global	0.93	0.94	1.7 mm day^{-1}
Air temperature at 2 m	Willmott and Matsuura 1950–99. Land	0.94	0.91	3.5 K
SWCRF	CERES 2000–03. Global	1.02	**0.90**	22.8 W m^{-2}
LWCRF	CERES 2000–03. Global	0.97	0.93	11.7 W m^{-2}
T	ERA-40 1980–2001. Global	0.84	**0.77**	2.1 K
RH	ERA-40 1980–2001. Global	0.78	**0.73**	11.0%
CBI		0.88	**0.82**	

can be affected by elevation differences between the model orography and reality. For the chosen fields, over most of the globe the differences between datasets are much smaller than the model errors. However, differences of less than 5% in rms error ratio may lie within the observational uncertainty for some fields.

Table 2 summarizes the error ratios for CAM3.5 and CAMUW. As documented by Neale et al. (2008), CAM3.5 is more skillful than CAM3.0 in simulating the Hadley circulation because of improvements in the deep cumulus parameterization. In particular, it shows reduced biases in sea level pressure (SLP), surface wind stress, zonal wind at 300 hPa, and temperature and RH. CAM3.5 also somewhat decreases the biases of surface rainfall and near-surface air temperature over land. However, it is less successful in reducing biases in cloud radiative forcings, especially for shortwave cloud radiative forcing (SWCRF). Its overall CBI is 0.88.

CAMUW has surprisingly small impacts on the rms error ratios considering its large differences from CAM3.5. The impacts on all fields except rainfall are positive, and the overall CBI improves to 0.82. The biases of SWCRF are most reduced, by 12%. Bias reductions of 5% or more are also achieved for SLP, upper-level zonal winds, and the three-dimensional structure of temperature and RH. Smaller but still significant bias reductions occur in longwave cloud radiative forcing (LWCRF), surface wind stress, and surface air temperature. We will compare the CAM3.5 and CAMUW simulations in more detail in the next section. We emphasize cloud- and PBL-related fields, which the UW schemes were designed to more skillfully simulate.

6. Discussion of CAMUW and CAM3.5 global climatology

a. CRF, LCA, LWP, and precipitation

Figures 3 and 4 compare annual-mean TOA SWCRF and LWCRF simulated by CAM3.5 and CAMUW with CERES satellite retrievals. Both simulations qualitative capture the major cloud regimes, with CAMUW having smaller overall rms errors, especially in SWCRF. CAM3.5 predicts both |SWCRF| and LWCRF relatively well in the oceanic storm tracks, but overpredicts |SWCRF| in the trade cumulus regimes and underpredicts |SWCRF| in the subtropical stratocumulus regions. In contrast, CAMUW slightly overpredicts the |SWCRF| contrast between the trade cumulus and subtropical stratocumulus regimes and overpredicts Northern Hemisphere storm-track |SWCRF|. The behavior of both simulations in the subtropical stratocumulus and trade cumulus regimes is consistent with the single-column studies of BOMEX (section 4) and nocturnal stratocumulus (BP09). At the coastal edges of the subtropical stratocumulus decks, both models underpredict |SWCRF|. This is likely in part due to inadequate horizontal resolution to capture land–ocean contrasts, as shown by BMG04.

Over most land areas, both models have similar bias patterns in both LWCRF and SWCRF. They underpredict both CRFs over the extratropical continents (except Australia). |SWCRF| is particularly underestimated over China. Both simulations also have similar bias patterns in LWCRF over the ocean, except for a weak decrease of LWCRF across the subtropics in CAMUW, and a stronger decrease in LWCRF in near-equatorial deep convection regions of the Pacific and Atlantic Oceans. The considerable similarities between the CAM3.5 and CAMUW bias patterns suggest the importance of other physical parameterizations (deep convection, stratiform cloud, and land surface) for controlling patterns of cloudiness.

SWCRF depends on the cloud fraction and cloud optical thickness. Figure 5 compares annual-mean low-cloud amount (LCA) from CAM3.5 and CAMUW with the Extended Edited Cloud Reports Archive (EECRA) climatology of routine surface observations (Hahn and Warren 1999). LCA is defined differently in simulations

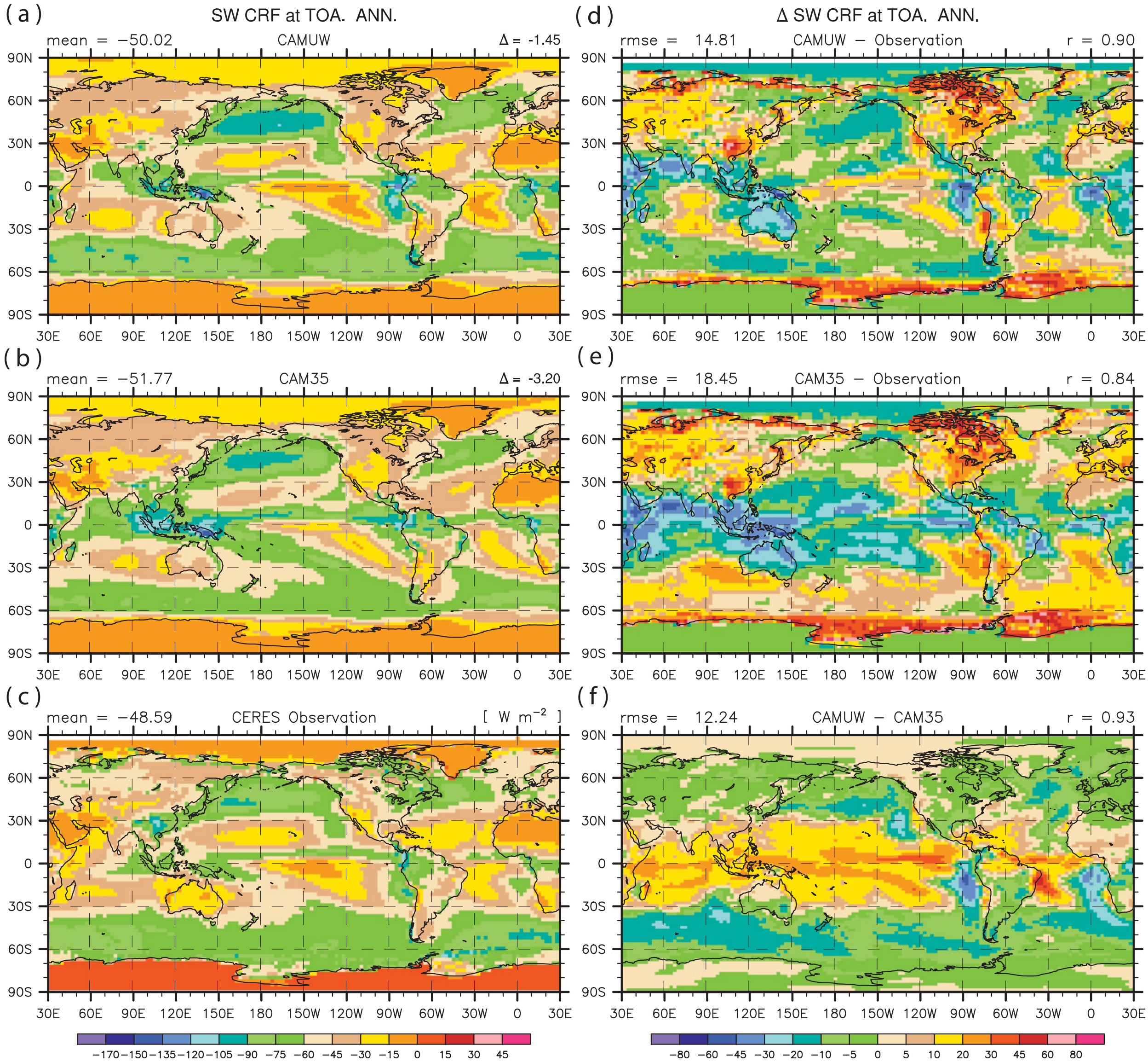

FIG. 3. Annual-mean climatologies of SWCRF from (a) CAMUW, (b) CAM3.5, and (c) CERES satellite "observations." Also shown are the differences of SWCRF between (d) CAMUW and observations, (e) CAM3.5, and observations, and (f) CAMUW and CAM3.5. Shown atop plots are (a)–(c) global mean values, and (d)–(f) spatial rms differences (rmse) and spatial correlation coefficients r between pairs of fields.

and observations and should not be blindly differenced: for simulations, LCA is defined as the aggregated cloud fraction between the surface and 700 hPa assuming maximum overlap, while the surface-observed LCA is defined as the cloud fraction with cloud base below 3000 ft, estimated by an observer based on whole-sky cover. In cumuliform cloud regimes, the whole-sky cloud cover can significantly exceed the column cloud cover. Qualitatively, both simulations reproduce the observed patterns of LCA with maxima in the midlatitude storm tracks and subtropical stratocumulus decks and minima in the trade cumulus regime over the ocean. The maxima are better simulated by CAMUW, while the minima are better simulated by CAM3.5. Since CAM3.5 artificially limits low-cloud cover in very dry air, it produces less LCA than CAMUW in the polar regions. However, the CRF difference between the models in these regions is small. A sensitivity simulation with the same low-cloud limiter in CAMUW produced similar LCA to CAM3.5 in the polar regions, but it marginally degraded the global simulation of SWCRF, as well as the overall climate bias index.

Figure 6 compares grid-column mean liquid water path (LWP) from the simulations with a 1987–2000

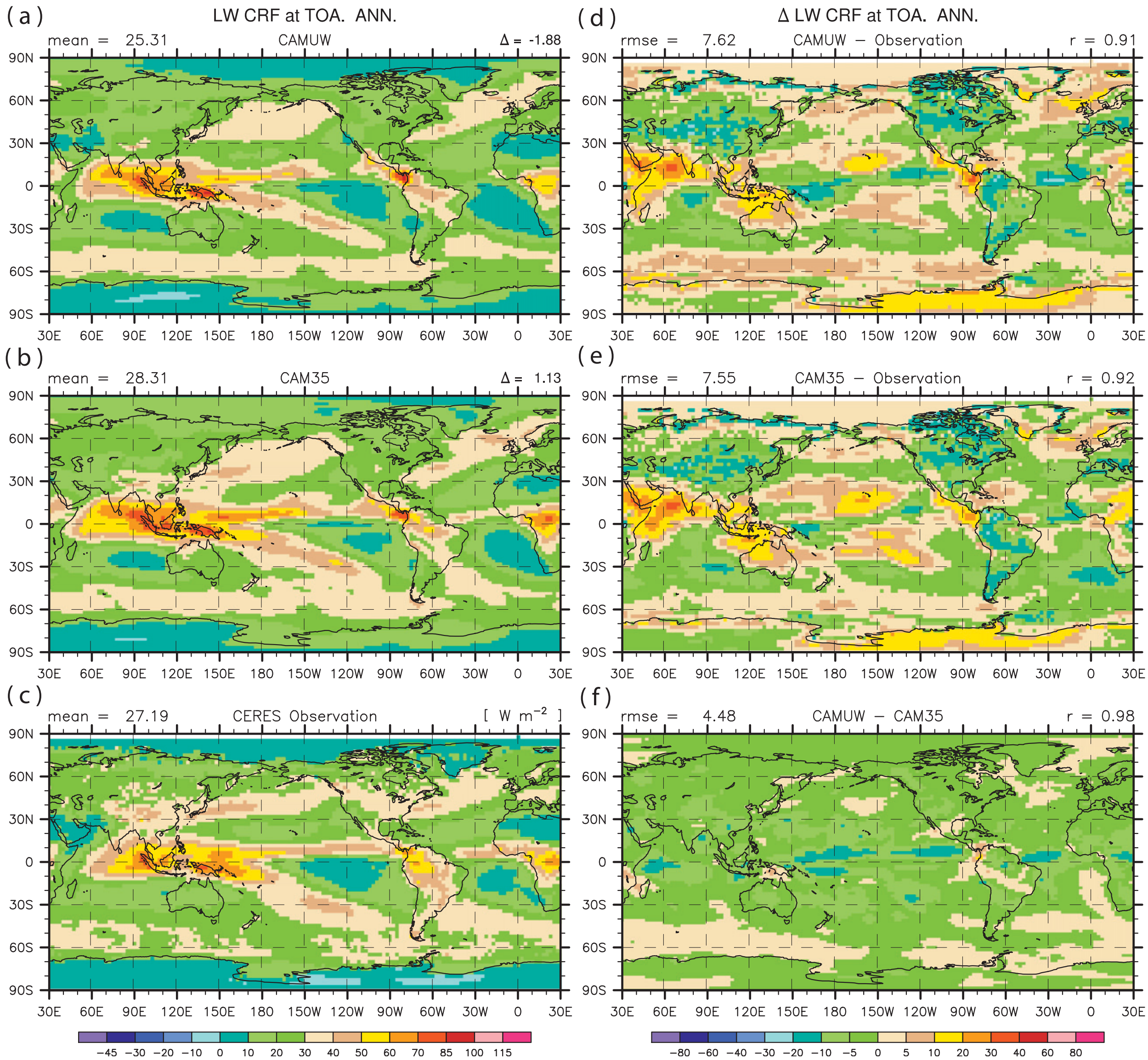

FIG. 4. As in Fig. 3, but for LWCRF.

mean LWP derived from the Special Sensor Microwave Imager (SSM/I) installed on several polar-orbiting satellites (Wentz 1997). Both simulations have very similar bias patterns, with too much LWP in the oceanic storm tracks and deep convection regimes and too little LWP in trade cumulus regions. The biases are more pronounced in CAMUW than CAM3.5. Of all the variables examined, LWP has the largest ratio of rms error to the observed standard deviation, with a global pattern correlation with the observation of only 0.4. The LWP anomaly has a very similar spatial pattern to the observed mean LWP: CAM tends to overestimate (underestimate) LWP where mean LWP is large (small). While there are some uncertainties in the SSM/I LWP satellite-retrieval algorithm, we attribute these biases primarily to CAM's stratiform cloud parameterization. In fact, changed stratiform microphysics has a large impact on this bias pattern (Gettelman et al. 2008), except in the trade cumulus regions. In the trade cumulus regions, the BOMEX single-column simulations (section 4) suggest that the cloudiness and liquid water biases may be mainly due to a poor reconstruction of the vertical liquid water profile in cumulus clouds by the stratiform scheme and perhaps also due to poor cloud overlap assumptions.

Figure 7 shows the rainfall biases simulated by CAM3.5 and CAMUW compared to GPCP, which are remarkably similar. We believe these biases are mainly

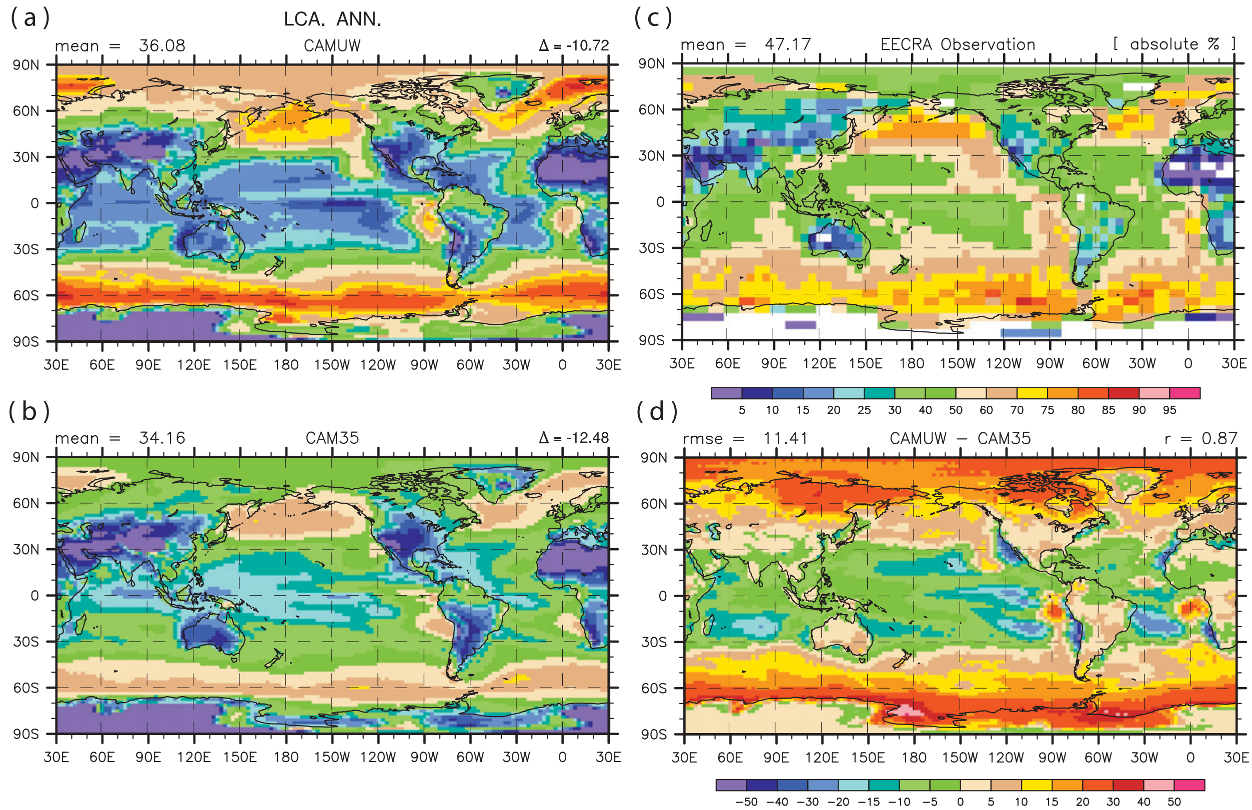

FIG. 5. As in Figs. 3a–c,f, but for LCA. Low cloud amount in simulations and observation is defined somewhat differently, as explained in the text.

driven by the deep convection scheme, since they are largest in the tropics. Wet and dry biases in the equatorial Pacific and western Indian Oceans correspond to anomalies in LWCRF seen on Fig. 4 in both simulations. This illustrates that cloud biases cannot be separated from circulation biases.

Figure 8 shows the CAMUW- and CAM3.5-simulated annually averaged shallow cumulus mass fluxes at a pressure roughly 0.94 of the surface pressure, or 60 hPa above the surface. This is typically just above the shallow cumulus cloud base over the low-latitude oceans. It is overlaid on EECRA surface observations of the annually averaged frequency of occurrence of shallow cumulus clouds (with CAMUW) and stratiform clouds (with CAM3.5). One sees a close correspondence between the CAMUW shallow cumulus mass flux and the observed shallow cumulus cloud occurrence: with a global pattern correlation of 0.88. However, shallow convective activity in CAM3.5 more resembles the pattern of stratiform clouds than shallow cumulus. This is consistent with the single-column nocturnal stratocumulus simulation of BP09, in which CAM3.5 shallow convection was very active in moist mixing and entrainment in the stratocumulus regime. Over the warmest oceans where deep convection is active, the shallow cumulus mass flux is smaller and has little impact on the CAM deep convection scheme.

b. Near-surface air temperature over land

Figure 9 plots the annual-mean near-surface temperature biases at 2-m height compared to the Willmott–Matsuura climatology. The simulated 2-m temperature is computed by interpolating between the surface and lowest grid-layer temperatures using the Monin–Obukhov stability functions. Overall, the biases are very similar in CAMUW and CAM3.5, implying that other factors (e.g., horizontal advection, cloud–radiation interaction, land surface properties) are controlling the biases. There is a tendency for CAMUW to be 1–2 K cooler than CAM3.5 at high latitudes, which reduces biases in some regions and increases them in others. This is consistent with different mixing structures in stable regimes between the two models: CAMUW does not allow turbulent mixing at gradient Richardson numbers exceeding 0.2 while CAM3.5 does, which should affect ''decoupling'' of land surface and free-tropospheric temperature in the strongly stable PBL common at high latitudes. While the biases against

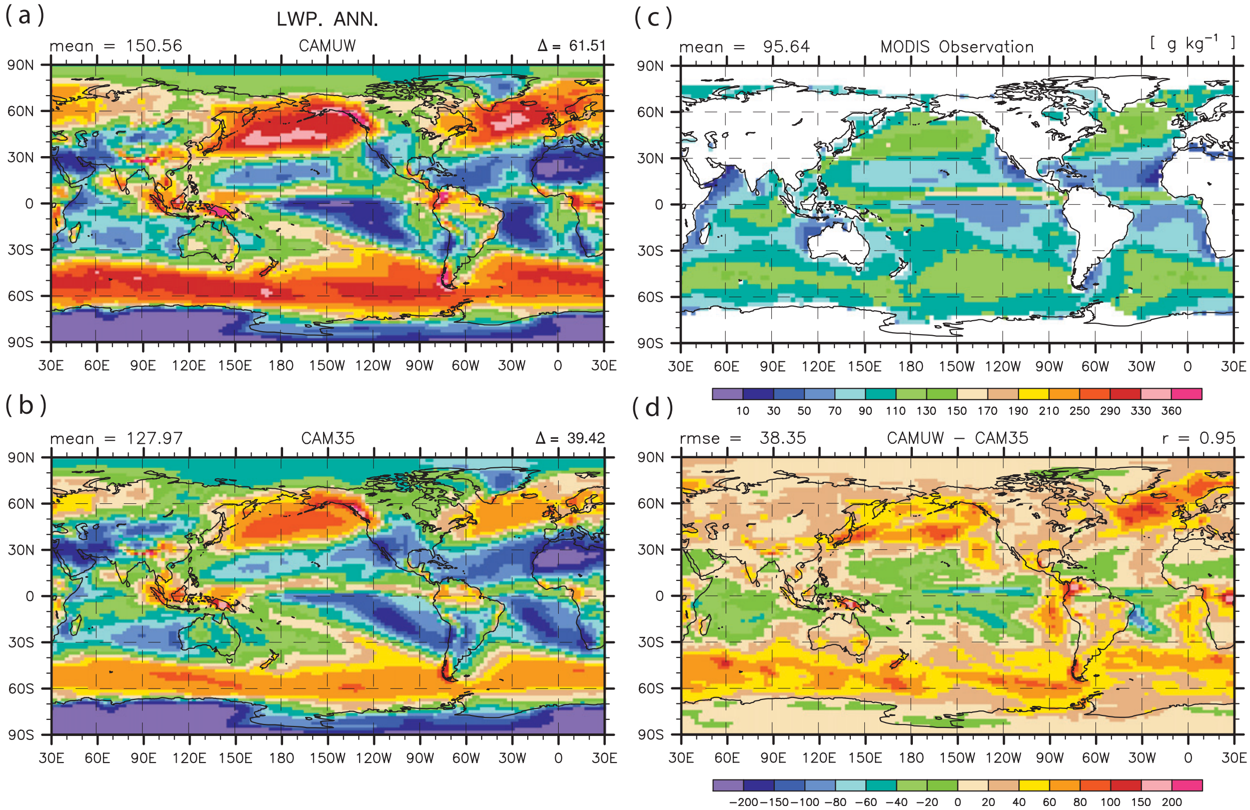

FIG. 6. As in Figs. 3a–c,f, but for grid-mean LWP.

observation have some seasonality, the differences between CAMUW and CAM3.5 are similar in DJF and JJA (not shown).

The land temperature biases are partly associated with cloud cover both in and above the boundary layer. In summer, the land temperature bias pattern in the extratropical Northern Hemisphere is correlated with the biases of net surface CRF ($r = 0.4$).

c. SLP and surface stress

Figure 10 plots the anomaly patterns of SLP and surface zonal wind stress in CAMUW compared to the observations. CAM3.5 (not shown) shows very similar anomaly patterns, suggesting these biases are not primarily induced by the PBL and shallow convection schemes. We also checked that this SLP bias pattern was insensitive to the parameters in our PBL or shallow convection schemes (e.g., the moist entrainment enhancement factor in the UW PBL scheme, and the shallow convective parameters in Table 1). Like earlier versions of CAM, both simulations have too strong subtropical highs, creating excessively strong easterly trade winds and midlatitude westerlies that create corresponding zonal wind stress anomalies.

The anomaly pattern of latent heat flux in both models (not shown) is similar to the pattern of stress anomaly, implying that it is controlled mainly by wind (as opposed to near-surface humidity) biases. CAMUW shows slightly larger latent heat fluxes (by <15 W m^{-2}) across most of the subtropical stratocumulus regions, consistent with slightly more entrainment mixing. Larger latent heat flux differences of both signs (locally up to 30 W m^{-2} in the western equatorial Pacific) are seen over the warmer oceans. These are probably due in large part to circulation differences between the simulations. CAMUW slightly increases the surface sensible heat flux (locally by up to 5 W m^{-2}) compared to CAM3.5 over the warmer tropical oceans, with little change in the stratocumulus regions. Multiple physical processes seem to contribute to these sensible heat flux differences.

We also found seasonal biases in synoptic storm-track activity in the midlatitude regions, which are correlated to the biases of CRFs there (not shown). These important biases have been reduced about 20% in CAM3.5 compared to earlier versions of CAM by improvements to the deep convection parameterization, and have been slightly further reduced through our changes, but need

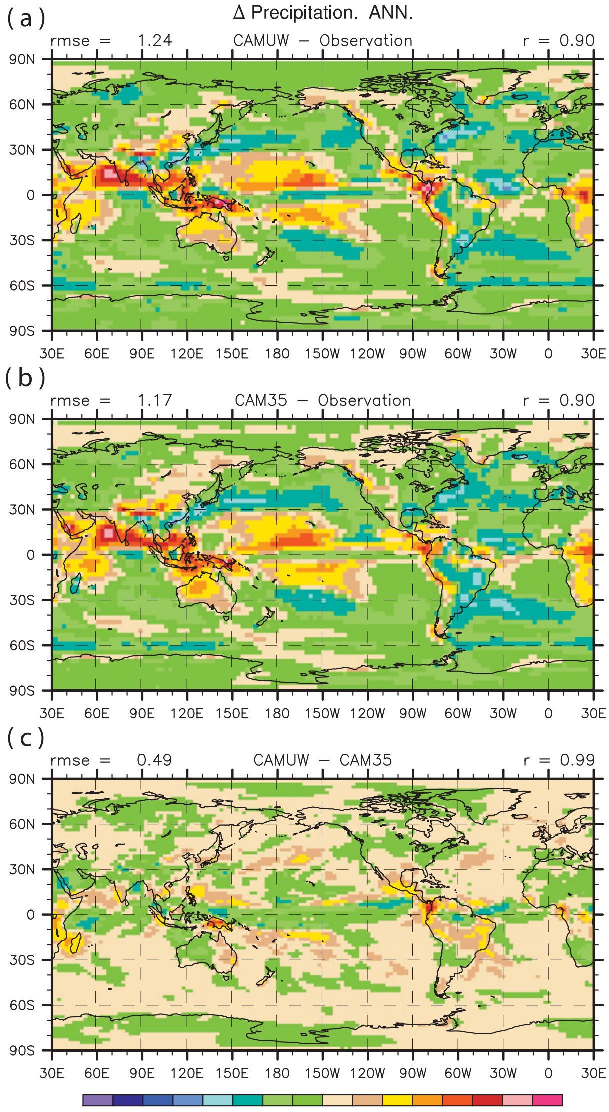

FIG. 7. As in Figs. 3d–f, but for precipitation rate (mm day^{-1}).

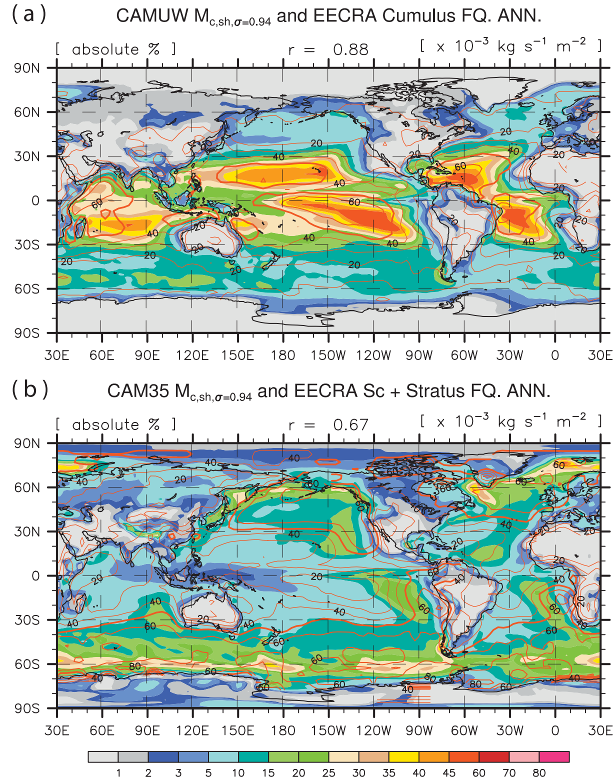

FIG. 8. Shallow convective updraft mass flux from (top) CAMUW and (bottom) CAM3.5 at σ = 0.94 with surface-observed frequency of shallow and moderate convective cloud (i.e., CL1,2; top), and stratocumulus and stratus cloud (i.e., CL6,5,8,4,7, bottom) contoured in red. Global pattern correlation between convective mass flux and observed cloud frequency are on top of each figure.

further attention. The high SLP bias in CAM is sensitive to the parameterizations of gravity wave drag and turbulent mountain stresses, especially during boreal winter (Y. Richter 2008, personal communication).

7. Vertical cross sections in subtropical stratocumulus to trade cumulus transition

Figures 11a–d show CAMUW-simulated vertical cross sections through the southeast Pacific stratocumulus region along 20°S, between the South American coast and 120°W. This is the steadiest and most persistent stratocumulus regime in the world. The cross sections are climatological averages for September–October–November, the season of maximum observed stratocumulus extent in this region.

The colors in Fig. 11c and the black contours in Fig 11d show cloud fraction and layer-mean liquid water content in each grid layer. The black contours in Fig. 11c show the shallow cumulus mass flux. We see a clear transition from stratocumulus near the coast to trade cumulus well offshore, marked by an offshore decrease in cloud cover and increase in cumulus mass flux. The heavy black lines in all panels show the diagnosed PBL height (which for CAMUW is the top grid interface of the lowest turbulent layer). The cumulus mass flux clearly originates and maximizes at the PBL top, as physically anticipated. Figure 11a shows the buoyancy production of the TKE and the TKE itself. These are large under the stratocumulus where the cloud-top longwave cooling is strong. Because the cloud layer is so shallow and its height varies in time, there is no clear maximum in buoyancy production at the mean height of the cloud layer.

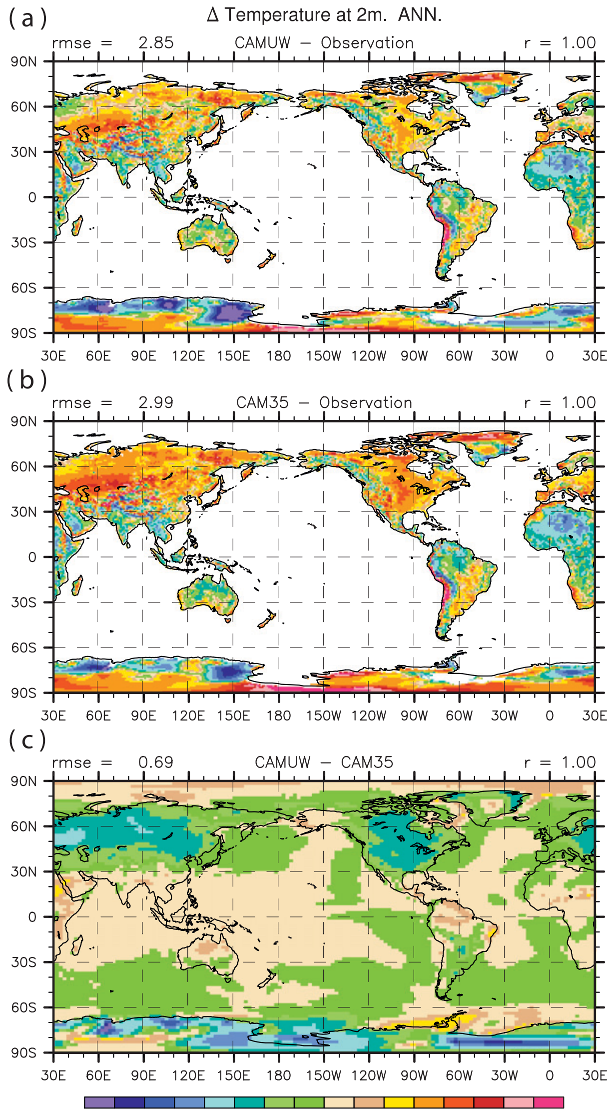

FIG. 9. As in Figs. 3e,f, but for 2-m air temperature (°C).

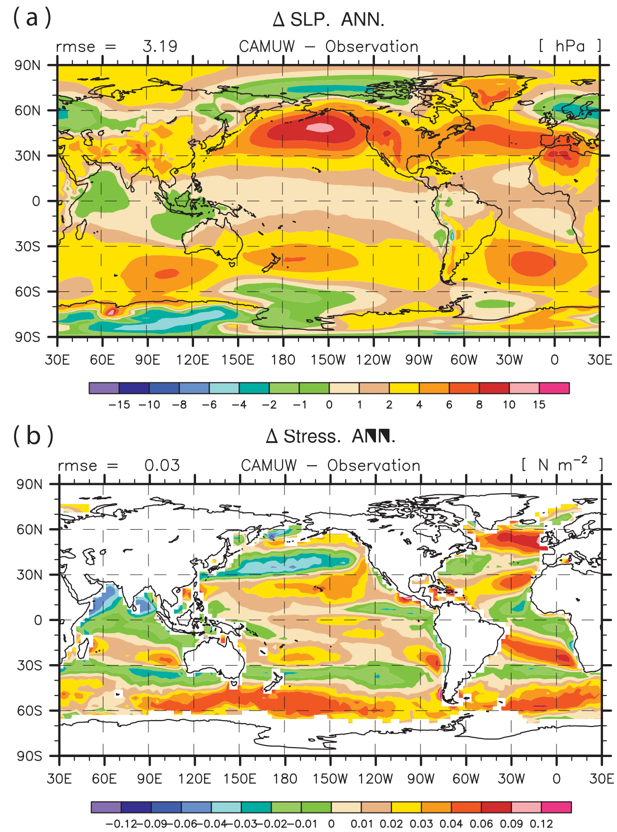

FIG. 10. Differences between CAMUW and observations for (a) SLP and (b) surface stress.

No clear transitional regime of cumulus under stratocumulus is simulated, as can be seen from the lack of elevated maxima cloud fraction (Fig. 11c) and buoyancy production (Fig. 11a) over the eastern edge of the shallow cumulus regime. This is the cause of the positive simulated SWCRF biases west of 95°W seen in Fig. 3d. With a lower value of the penetrative entrainment parameter (rpen = 5 rather than rpen = 10), we can greatly improve the simulation of the stratus-under-cumulus transition both here and in the northeast Pacific (not shown), but only at the expense of undesirably intensifying SWCRF in the storm tracks.

The CAMUW θ and q cross sections (colors in Figs. 11b,d) show the expected structure, with a fairly well-mixed layer below the mean PBL height, a cumulus layer west of 95°W with some vertical gradients of θ and q, and a sloped trade inversion visible as a layer of stronger vertical gradients of θ and q, capped by warm, dry air. The white contours indicate biases of θ and q with respect to ERA-40. There is a warm, dry bias (Figs. 11b,d) above the simulated inversion near the coast, showing that the mean trade inversion is somewhat too shallow there compared to ERA-40, which may already be biased toward a low inversion in this region—see Bretherton et al. (2004b). Satellite-derived cloud-top-height climatologies (e.g., Wood and Bretherton 2004) suggest that at 20°S the trade inversion should remain above 1 km all the way to the coast. This bias seems to be due to underentrainment more than subsidence—the CAMUW 850-hPa ω (black contours in Fig. 11b) does not show a corresponding bias of excess subsidence compared to ERA-40. A separate short-term forecast test also showed that both CAMUW and CAM3.5 shallow down the PBL depth without excessive subsidence (Hannay et al. 2009). However, the CAMUW dry–warm bias above the stratocumulus region extends above 700 hPa, and may also reflect dynamics biases connected with the excessively strong subtropical

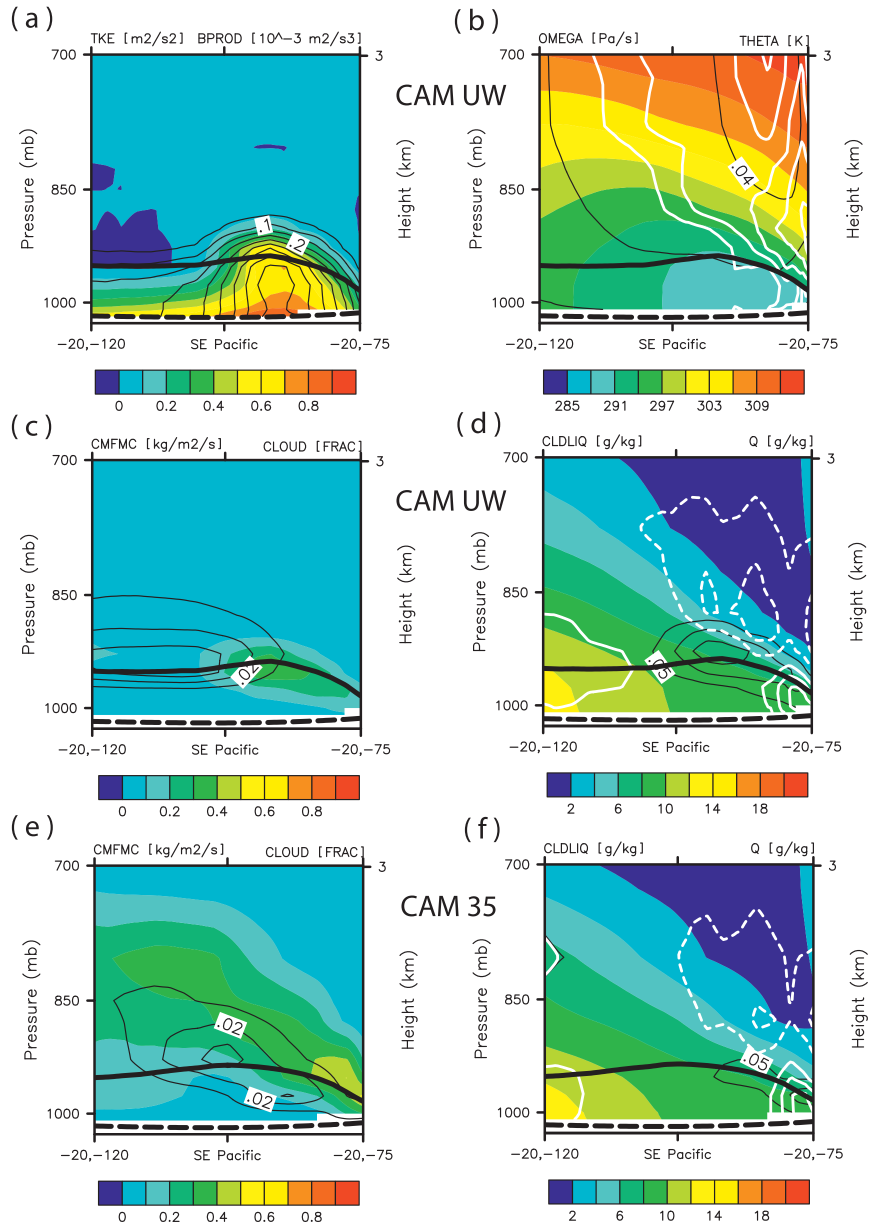

FIG. 11. Cross-sectional plots of (a)–(d) CAMUW-simulated and (e),(f) CAM3.5-simulated clouds and related environmental variables along 20°S over the southeast Pacific during SON. In each panel, the color-shaded and contoured fields are labeled at the upper right and left, respectively. The thick solid line in each panel indicates PBL top pressure, and the dashed line shows the mean surface pressure. BPROD is the buoyancy production of TKE. Contour interval is 0.02 Pa s^{-1} for ω, 0.05 g kg^{-1} for cloud liquid water content, 0.05 m^2 s^{-2} for TKE, and 0.01 kg m^2 s^{-1} for updraft mass flux (CMFMC) of the shallow cumulus scheme. The model biases against ERA-40 are also contoured (positive: solid white; negative: dotted white) in (b) for θ (1-K interval) and in (d) and (f) for q_v (1 g kg^{-1} interval).

high. These biases are found in all the subtropical stratocumulus regimes.

While it is possible to modify the UW moist turbulence scheme to deepen stratocumulus-capped boundary layers, this also tends to increase surface evaporation. Since the subtropical trades are too strong, a realistic surface humidity leads to excessive latent heat fluxes and an overly strong tropical Hadley circulation. This might further strengthen the subtropical high and counteract PBL deepening. Thus, unless other climate components are harmonized, changes that improve the vertical structure of subtropical cloud-topped PBL in our schemes can reduce compensation of other model biases and worsen the overall simulation. This suggests that reduction of CAM's SLP biases could allow further improvements of our simulation of the marine cloud-topped PBL.

Figures 11e,f shows analogous results for CAM3.5. CAM3.5 produces much more cloud fraction than CAMUW (Fig. 11e). The cloud tends to occur above the maximum in shallow cumulus mass flux. Thus, it seems to be associated with detrainment from the Hack shallow convection scheme, which is active all the way into the coast. However, there is much less cloud liquid water content in the stratus region than in CAMUW, causing underestimation of the magnitude of SWCRF in this region (Fig. 3e). Figure 11f also shows that CAM3.5 has a roughly similar dry bias to CAMUW at 900 hPa near the coast compared to ERA-40, indicating that it similarly underestimates inversion height in this region. Correspondingly, CAM3.5, like CAMUW, is too moist within the PBL near the coast. Figure 11e shows that CAM3.5's cloud cover at the lowest grid level is 0.2–0.4 within 300 km of the coast, implying frequent fog in a region in which this is not observed.

We have chosen to present the southeast Pacific cross section because the large-scale dynamics in this region are well represented in CAM, so model biases are probably due mainly to the moist physics parameterizations. We have done a similar analysis along a northeast Pacific cross section from San Francisco to Hawaii. Here CAMUW and CAM3.5 exhibit stronger subsidence than ERA-40 near the coast, so the cloud biases could also have a dynamical contribution. However, we find that the biases of both CAMUW and CAM3.5 are similar to the southeast Pacific, suggesting that moist physics parameterizations are still the main source of model error in the simulated northeast Pacific cloud-topped boundary layer.

8. Summary and conclusions

We have modified the UW shallow convection scheme for GCM applications with a large integration time step and coarse vertical resolution. Our scheme is implemented along with a new UW moist turbulence scheme into CAM3.5 and compared with the default turbulent mixing and shallow convection schemes.

Compared to CAM3.5, CAMUW has several conceptual advantages. It is designed to produce convergent results at high vertical and time resolution. It is based fully on moist conservative variables appropriate for simulation of saturated thermodynamics. The moist turbulence scheme can respond appropriately at any model level to internal destabilization of the atmosphere, while the CAM3.5 PBL scheme directly responds only to destabilization of the PBL by surface fluxes. The CAMUW does not require the regime-specific empirical schemes used in CAM3.5 for specifying low-cloud fraction for stratocumulus under strong inversions and for Arctic stratus. The entrainment parameterization of the UW moist turbulence scheme and the updraft microphysics of the UWShCu scheme can be easily extended to allow for the effect of aerosols on these processes. Last, the CAM3.5 shallow cumulus scheme is also instrumental in moist turbulent mixing, such as stratocumulus entrainment, which has different physical characteristics than cumulus convection. In CAMUW, moist turbulence and shallow cumulus convection occur in the physically expected places, and the CAMUW parameterizations perform better than those in CAM3.5 in GCSS single-column tests for simulating boundary layer cloud, while maintaining a simulation of dry stable and convective boundary layers that is at least as good as in, or superior to, CAM3.5. A single-column test of nonprecipitating shallow convection shows that CAMUW produces a more realistic vertical structure of thermodynamic and cloud variables with much less sensitivity to vertical resolution than CAM3.5.

To measure global performance, we introduced a suite of global metrics of how well the simulated climate and its seasonal cycle match observations, and synthesized these into a climate bias index, scaled such that CAM3.0 would score 1.00. CAM3.5 already improves the CBI to 0.88; CAMUW further improves it to 0.82. The greatest improvement of CAMUW biases over CAM3.5 (12%) occurred in SWCRF because of the improved simulation of subtropical marine boundary layer clouds. Biases of SLP, upper-level winds, temperature, and relative humidity are also reduced more than 5%, along with slightly smaller bias reductions in surface wind stress, air temperature, and LWCRF. The cloud forcing improvements in CAMUW occur despite a slight amplification of large CAM3.5 biases in LWP. The new microphysics scheme of Gettelman et al. (2008) greatly reduces these biases. Surface rainfall biases, as well as the pattern of surface air temperature biases, are rather insensitive to our changes of parameterization and vertical resolution. This suggests that other physical parameterizations—including the deep convection, gravity wave drag, and land surface schemes—may be controlling these biases. CAMUW simulations coupled to a dynamic ocean, to be reported on separately, also have similar climatological bias patterns in most fields to the specified-SST simulations reported here.

To fully realize the potential benefits of the UW moist turbulent and shallow convection schemes, we are working with colleagues in the Community Climate System Model (CCSM) Atmospheric Model Working Group on developing a stratiform cloud scheme with an improved interface to shallow convection. We are also striving to develop our shallow cumulus scheme into a unified parameterization that can also realistically parameterize deep convection and to refine various aspects of our moist turbulence scheme.

Acknowledgments. We would like to acknowledge support from the NASA EOS program through Grant NNG05GA19G and the DOE ARM program through Grant DE-FG02-05ER63959. This paper was made possible because of the earlier work of Ping Zhu; help from Phil Rasch, Dani Coleman, Cecile Hannay, and Rich Neale in working with the CAM; diagnostics help from Matt Wyant and Mark Stevens; and LES simulations from Peter Blossey using the System for Atmospheric Modeling provided by Marat Khairoutdinov.

APPENDIX

Revised University of Washington Shallow Convection Scheme

In this appendix, we summarize important modifications made to the UW shallow cumulus scheme since the initial development by BMG04. Note that the index in this appendix and Fig. 1 for the UW convection scheme increases upward, which is opposite to that of the accompanying manuscript on the UW moist turbulent scheme (BP09).

a. Implementation of implicit CIN

The CIN is defined as the vertically integrated buoyancy of undiluted cumulus updraft from the PBL top to the level of free convection (LFC; see Fig. 1). Along with mean PBL TKE e, CIN determines cumulus updraft mass flux in our parameterization:

$$M = 0.4\rho\sqrt{e}\exp\left(-\frac{\mathrm{CIN}}{e}\right). \tag{A1}$$

CIN is sensitive to small changes in the column thermodynamic profiles. In reality, the strong negative feedback of CIN on cumulus mass flux creates a very stable relationship between these two variables. However, a standard forward-difference discretization of this ‘‘stiff’’ feedback and a sufficiently large time step can lead to unstable oscillations in CIN that lead to on–off switching of the convection between time steps. To stabilize this feedback, we now diagnose mass flux based on ‘‘implicit’’ CIN computed using thermodynamic profiles at the end of the time step rather than ‘‘explicit’’ CIN computed using thermodynamic profiles at the beginning of the time step, analogous to using a backward-Euler instead of a forward-Euler discretization of a stiff ordinary differential equation. We can implement *implicit* CIN with minimum computational cost using the following predictor–corrector algorithm.

Let superscript 0 denote a value corresponding to the input thermodynamic profile to UWShCu. The shallow cumulus tendencies of the profiles are the product of a mass flux and a normalized tendency per unit mass flux (which is computed from the input state). Let CIN^0 be the explicit CIN computed from the input profile and M^0 be the corresponding cumulus mass flux from our mass-flux closure. Let 1 denote a value after the profiles have been evolved forward Δt using the mass flux M^0. This evolved profile will have a CIN^1, which will usually exceed CIN^0, since the compensating subsidence from cumulus convection should help warm and dry the environment near the cloud base. If we used CIN^1 in the mass-flux closure, we would get less mass flux than M^1.

Our goal is to find a reduced implicit mass flux $M^* = \alpha M^0$ $(0 \le \alpha \le 1)$ for which the mass-flux closure holds at the end of the time step, to prevent overstabilization and instability of the system with long time steps. Let * denote a value after the profiles have been evolved forward Δt using the mass flux M^*. Since thermodynamic tendencies are proportional to the mass flux, it becomes $\overline{\theta_v^*} = \overline{\theta_v^0} + \alpha(\overline{\theta_v^1} - \overline{\theta_v^0})$, and the definition of CIN implies

$$\mathrm{CIN}^* \equiv \frac{1}{\rho\theta_{\mathrm{ref}}} \cdot \int_{p_{\mathrm{TOP}}}^{p_{\mathrm{LFC}}} (\theta_{v,u} - \overline{\theta_v^*})dp = \mathrm{CIN}^0 + \alpha\Delta\mathrm{CIN}, \tag{A2}$$

where $\Delta\mathrm{CIN} \equiv \mathrm{CIN}^1 - \mathrm{CIN}^0$, θ_{ref} is reference potential temperature, p_{LFC} is LFC, p_{TOP} is PBL top, and $(\theta_{v,u}, \overline{\theta_v},)$ are virtual potential temperatures of undiluted cumulus updraft and environment. For simplicity, we neglect variations o f p_{LFC}, p_{TOP}, and $\theta_{v,u}$ during time marching. If $\Delta\mathrm{CIN} < 0$, we just use the explicit CIN $(\alpha = 0)$. Otherwise, from the mass-flux closure,

$$\begin{aligned} M^1 &= 0.4\rho\sqrt{e}\exp\left(-\frac{\mathrm{CIN}^1}{e}\right), \\ M^* &= \alpha M^0 = 0.4\rho\sqrt{e}\exp\left(-\frac{\mathrm{CIN}^*}{e}\right). \end{aligned} \tag{A3}$$

From the above three equations, we can derive

$$\alpha = \exp\left(-\alpha\frac{\Delta\mathrm{CIN}}{e}\right). \tag{A4}$$

Since $\Delta\mathrm{CIN} \geq 0$, a unique solution of α between 0 and 1 is guaranteed. Once α is obtained, CIN* and M^* can be calculated and profiles can be implicitly marched.

b. Reconstructed PBL top and convective fluxes within PBL

The treatment of fluxes within the PBL below the shallow cumulus layer has been heavily modified from BMG04. The shallow cumulus updraft initiates from the top of the PBL. In the UW moist turbulence scheme, the PBL is defined as the lowest turbulent regime adjacent to the surface. Under shallow convection, the PBL is almost invariably a convective layer, and the PBL "top" is defined as its top flux interface. The "ambiguous" grid layer just above the PBL top is visualized as being a partial grid layer of above-PBL air atop and another partial grid layer of PBL air. The fraction of PBL air in this layer can be reconstructed by comparing its mean thermodynamic properties with those of the PBL and those of the overlying grid layer—this is used to specify the PBL top for UWShCu, which can vary continuously between model grid interfaces, allowing smooth transition of the system. We also visualize cumulus updrafts as "ventilating" mass from below this PBL top in the ambiguous layer. Thus cumulus mass fluxes are coupled to the PBL in large part though their effects on the ambiguous layer. Ideally, CIN should also be computed from the reconstructed PBL top, but this would complicate the code and probably have little effect on the results. Hence we keep the original implicit CIN.

To calculate heat, moisture, and momentum fluxes due to shallow cumulus in and below the ambiguous or inversion layer I, we first reconstruct the PBL-top inversion within this layer. Let a_I be the layer-mean value of a conservative scalar (e.g., $a = q_t, \theta_l, u, v$) in the layer I. Let $a_{I+1/2}$ and $a_{I-1/2}$ be interface values just above and below layer I, which are assumed to characterize the above-PBL and PBL air within the layer (see Fig. 1). Then a reconstructed PBL top pressure p_{inv} for a is calculated such that that the layer-mean value of a matches a_I:

$$p_{\mathrm{inv}} = p_{I-1/2} - r|\Delta p_I|, \quad r = \left(\frac{a_I - a_{I+1/2}}{a_{I-1/2} - a_{I+1/2}}\right), \tag{A5}$$

where $|\Delta p_I|$ is the pressure thickness of layer I.

The cumulus updraft mass flux draws down the reconstructed PBL top. If the cumulus updrafts started with the same properties as the PBL air within the ambiguous layer, there would be no cumulus fluxes below the ambiguous layer. However, this is not the case. To avoid over stabilizing or destabilizing the ambiguous layer and PBL through cumulus ventilation, we remove the necessary additional flux equally throughout the whole PBL, which results in the following ShCu flux at interfaces below p_{inv}:

$$(\overline{\omega' a'})(k) = gM(a_{\mathrm{src}} - a_{I-1/2})\left(\frac{p_{1/2} - p_k}{p_{1/2} - p_{\mathrm{inv}}}\right), \quad \text{for} \quad 1/2 \leq k \leq I - 1/2, \tag{A6}$$

where ω is pressure vertical velocity, the subscript "SRC" refers to the cumulus updraft source air, and $p_{1/2}$ is the surface pressure.

There is one additional possible complication because of the finite length of a time step. It is possible for compensating subsidence associated with cumulus updraft mass flux to lower the PBL top below the bottom of the ambiguous layer, in which case compensating subsidence will also warm and dry the grid layer below. To diagnose whether compensating subsidence would lower p_{inv} below $p_{I-1/2}$ during Δt, we compare the normalized cumulus updraft mass flux, $r_c = (gM\Delta t)/|\Delta p_I|$, to r. If $r_c > r$, p_{inv} will be lowered down into layer $I - 1$, replacing PBL-top air with $a = a_{I-1/2}$ with above-PBL air with $a = a_{I+1/2}$. This effect is included by adding a flux $-gM(a_{I+1/2} - a_{I-1/2})\,(1 - \mathrm{r}/\mathrm{r_c})$ to $(\overline{\omega' a'})(k = I - 1/2)$ for $r_c > r$.

The above derivation assumes that cumulus mass flux is not strong enough to lower down p_{inv} below $p_{I-3/2}$, that is, $gM\ \Delta t < r|\Delta p_I| + |\Delta p_{I-1}|$. For a GCM simulation with $\Delta t = 1800$ s, this roughly corresponds to $M < 0.2$ kg m^{-2} s^{-1}, which is much larger than typical values of M. For safety, we impose an upper bound on the cumulus-base mass flux of $gM\ \Delta t < 0.9|\Delta p_{I-1}|$, so the above derivation is always valid. However, for use of our scheme at higher vertical resolution, a smaller Δt should be chosen to avoid widespread triggering of this limiter. We applied this ShCu flux algorithm separately to each conservative scalar (q_t, θ_l, u, v); the reconstructed inversion need not be the same for all scalars.

c. Revised buoyancy sorting

A few changes have been made to the buoyancy-sorting algorithm used by BMG04 to calculate the entrainment and detrainment rates, which many studies have noted are critically important for controlling cumulus updraft properties. In BMG04, these rates scale with a specified lateral mixing rate ε_o (Pa^{-1}), which BMG04 assumed is constant with height and inversely proportional to the cumulus-top height depth. Based on a suggestion of Stephan de Roode and Pier Siebesma, we now parameterize ε_o as an inverse function of geometric height as

$$\epsilon_o = \frac{c}{\rho g z}. \tag{A7}$$

The nondimensional constant $c = 8$ was fitted to an LES simulation of the BOMEX case (Siebesma et al. 2003).

In BMG04, a uniform spectrum of mixtures of updraft and environmental air is assumed. Only mixtures with positive buoyancy or vertical velocity strong enough to rise at least a certain distance are entrained. BMG04 added a further restriction that only saturated mixtures should be entrained into the cumulus updraft. This can cause excessive cumulus updraft velocity compared to LES. Thus, in UWShCu, nonsaturated as well as saturated mixtures are entrained as long as they have positive buoyancy or sufficient strong vertical velocity to satisfy the BMG04 entrainment criterion.

d. *Other changes*

- The source air properties of the cumulus updraft have been slightly modified based on LES comparisons: its humidity $q_{t,\mathrm{src}}$ is that of the lowest model layer, $\theta_{\mathrm{vl,src}}$ is the minimum θ_{vl} over all model layers within the PBL, $\theta_{l,\mathrm{src}}$ is computed from $q_{t,\mathrm{src}}$ and $\theta_{\mathrm{vl,src}}$, and (u_{src}, v_{src}) are taken from the top model level within the PBL.
- In computing turbulent fluxes at interfaces between the PBL top and the updraft LCL, we assume no lateral mixing between the cumulus updraft and the environment.
- If the cumulus updraft cannot reach to the "diluted" LFC (see Fig. 1), shallow cumulus convection is not performed. This can occasionally happen since CIN is computed up to the LFC using an undilute cumulus plume, while buoyancy sorting in the updraft plume occurs above the LCL. The effect of nonbuoyant "cumulus convection" is treated by our PBL scheme through the entrainment parameterization at the PBL top.
- UWShCu, unlike BMG04, treats evaporation of convective precipitation above cloud base, as in the CAM3 implementation of the Zhang–MacFarlane deep cumulus scheme (section 4.3 of http://www.ccsm.ucar.edu/models/atm-cam/docs/description/), which relates the vertical profile of rain evaporation rate E (s^{-1}) to the vertical profiles of grid-mean relative humidity RH and the precipitation flux R ($\mathrm{kg\,m^{-2}\,s^{-1}}$):

$$\begin{aligned} E &= K_e(1 - \mathrm{RH})R^{1/2}, \\ K_e &= 0.2 \times 10^{-5}[(\mathrm{kg\,m^{-2}\,s^{-1}})^{-1/2}\mathrm{s}^{-1}]. \end{aligned} \tag{A8}$$

Comparison of vertical profiles of precipitation flux with LES based on an ongoing GCSS precipitating trade cumulus case suggests that the coefficient K_e used in the deep convection scheme is also adequate for shallow cumulus.

- CAM's stratiform macrophysics and radiation schemes require specification of a shallow cumulus cloud fraction and a condensate detrainment rate at each level. Following BMG04, we compute a cumulus updraft fractional area $A_{u,k} = M_k/(\rho w_k)$ at each interface k in the Cu layer. LES of shallow cumulus ensembles (e.g., Siebesma et al. 2003) suggest that about 50% of the cloud cover at a given level is buoyant updraft, so we compute the overall shallow cumulus cloud fraction at interface k as $A_{\mathrm{shCu},k} = \nu A_{u,k}$, where the parameter $\mu = 2$.
- As in BMG04, detrainment of nonprecipitating cloud liquid and ice water is assumed to be proportional to the total water detrainment, assuming the detrained air is representative of cumulus updraft:

$$\begin{aligned} &D_{q_l} = (q_{l,u}/q_{c,u})D_{q_c},\ D_{q_i} = (q_{i,u}/q_{c,u}) \cdot D_{q_c}, \\ &q_{c,u} = q_{l,u} + q_{i,u}. \end{aligned} \tag{A9}$$

e. *Tunable coefficients in UWShCu and their ranges*

This section justifies the plausible ranges of the UWShCu tuning coefficients given in Table 1.

1) UPDRAFT LATERAL MIXING EFFICIENCY C

We based our choice $c = 8$ on BOMEX, for which the cumulus layer was only 1.5 km deep. Cloud-resolving simulations of precipitating tropical oceanic deep convection imply smaller values of $c \approx 2$–3, perhaps because of the boundary layer updrafts become broader when organized by cold pool dynamics (Kuang and Bretherton 2006). By decreasing c, one can make UWShCu more resemble a deep convection scheme. To avoid competition between UWShCu (used as a shallow cumulus scheme) and a separate deep convection scheme, it is therefore advisable not decrease c below 4. We feel it is legitimate to "tune" c in the range 4–8 to optimize a climate simulation, though we have not ourselves tried to do this.

2) PENETRATIVE ENTRAINMENT EFFICIENCY R_{PEN}

This parameter regulates the ratio of penetratively entrained air mass to the air mass detrained from cumulus updrafts in the overshooting zone above the level of neutral buoyancy (LNB). Because cumulus updrafts can keep churning and eddying above their LNB, even though their rise rate rapidly reduces, it is reasonable to assume $r_{\mathrm{pen}} > 1$. Our choice $r_{\mathrm{pen}}=10$ follows BMG04, who made this choice to optimize single-column simulations of a stratocumulus to trade cumulus transition.

Larger values of r_{pen} tend to produce too weak a capping inversion on trade cumulus layers in single-column simulations. Because this choice was not made on first principles, we regard any value between these two extremes as plausible.

3) Maximum core updraft fraction $A_{U,MAX}$

In UWShCu, the shallow cumulus *core* updraft fraction is not allowed to exceed $A_{u,\max} = 0.1$ at any level. Since cumulus updraft fractional area is about twice of the core updraft fractional area, cumulus updraft fractional area should not exceed 0.2 by this constraint. This limit is consistently enforced in the calculation of cumulus updraft mass flux, entrainment, and detrainment into the updraft. The limit is arbitrary and ideally should be taken large enough not to affect the simulation. Currently, it does somewhat affect the simulation in the stratocumulus to trade cumulus transition region. A larger value of $A_{u,\max}$ will increase cumulus activity and somewhat decrease overall cloud cover in these regions. We recommend that $A_{u,\max}$ can be used as a tuning parameter in the range 0.05–0.15. If the cumulus core updraft fraction exceeds 0.15, the convection is arguably better represented as a stratocumulus layer and should be handled by the moist turbulence scheme.

4) Maximum cumulus updraft condensate $Q_{C,MAX}$

In UWShCu, following BMG04, if the cloud condensate mixing ratio exceeds $q_{c,\max} = 1$ g kg^{-1}, all the excessive condensate is converted into precipitation. This threshold seems to match the mean cumulus updraft properties derived from our analysis of LES of shallow and even deep convection. It should probably be made dependent on cloud-nucleating aerosol properties, especially for simulation of aerosol indirect effects on climate, but we have yet to experiment with this. Because direct observations of in-cloud-condensate profiles averaged over the entire ensemble of cumulus updrafts are not readily available, and because LES microphysics is far from perfect, we regard $q_{c,\max}$ as a legitimate tuning parameter within the range 0.5–1.5 g kg^{-1}.

REFERENCES

Adler, R. F., and Coauthors, 2003: The Version-2 Global Precipitation Climatology Project (GPCP) Monthly Precipitation Analysis (1979–present). *J. Hydrometeor.,* **4,** 1147–1167.

Bentamy, A., Y. Quilfen, F. Gohin, N. Grima, M. Lenaour, and J. Servain, 1996: Determination and validation of average wind fields from ERS-1 scatterometer measurements. *Global Atmos. Ocean Syst.,* **4,** 1–29.

Bretherton, C. S., and S. Park, 2009: A new moist turbulence parameterization in the Community Atmosphere Model. *J. Climate,* **22,** 3422–3448.

——, J. R. McCaa, and H. Grenier, 2004a: A new parameterization for shallow cumulus convection and its application to marine subtropical cloud-topped boundary layers. Part I: Description and 1D results. *Mon. Wea. Rev.,* **132,** 864–882.

——, T. Uttal, C. W. Fairall, S. Yuter, R. Weller, D. Baumgardner, K. Comstock, and R. Wood, 2004b: The EPIC 2001 stratocumulus study. *Bull. Amer. Meteor. Soc.,* **85,** 967–977.

Brown, A. R., and Coauthors, 2002: Large-eddy simulation of the diurnal cycle of shallow cumulus convection over land. *Quart. J. Roy. Meteor. Soc.,* **128,** 1075–1093.

Collins, W. D., and Coauthors, 2006: The formulation and atmospheric simulation of the Community Atmosphere Model Version 3 (CAM3). *J. Climate,* **19,** 2144–2161.

GAMDT, 2004: The new GFDL global atmosphere and land model AM2/LM2: Evaluation with prescribed SST simulations. *J. Climate,* **17,** 4641–4673.

Gettelman, A., H. Morrison, and S. J. Ghan, 2008: A new two-moment bulk stratiform cloud microphysics scheme in the Community Atmospheric Model, Version 3 (CAM3). Part II: Single-column and global results. *J. Climate,* **21,** 3660–3679.

Gleckler, P. J., K. E. Taylor, and C. Doutriaux, 2008: Performance metrics for climate models. *J. Geophys. Res.,* **113,** D06104, doi:10.1029/2007JD008972.

Gregory, D., R. Kershaw, and P. M. Inness, 1997: Parameterization of momentum transport by convection. II: Tests in single column and general circulation models. *Quart. J. Roy. Meteor. Soc.,* **123,** 1153–1184.

Hack, J. J., 1994: Parameterization of moist convection in the National Center for Atmospheric Research Community Climate Model (CCM2). *J. Geophys. Res.,* **99,** 5551–5568.

Hahn, C. J., and S. G. Warren, 1999: Extended edited synoptic cloud reports from ships and land stations over the globe, 1952–1996. Rep. NDP026C, Carbon Dioxide Information Analysis Center, Oak Ridge National Laboratory, Oak Ridge, TN, 71 pp. [Available from Data Support Section, National Center for Atmospheric Research, Boulder, CO 80307-3000.]

Hannay, C., D. L. Williamson, J. J. Hack, J. T. Kiehl, J. G. Olson, S. A. Klein, C. S. Bretherton, and M. Koehler, 2009: Evaluation of forecasted Southeast Pacific stratocumulus in the NCAR, GFDL, and ECMWF models. *J. Climate,* in press.

Holtslag, A. A. M., and B. A. Boville, 1993: Local versus nonlocal boundary layer diffusion in a global climate model. *J. Climate,* **6,** 1825–1842.

Kain, J. S., and J. M. Fritsch, 1990: A one-dimensional entraining/detraining plume model and its application in convective parameterization. *J. Atmos. Sci.,* **47,** 2784–2802.

Khairoutdinov, M. F., and D. A. Randall, 2003: Cloud resolving modeling of the ARM summer 1997 IOP: Model formulation, results, uncertainties, and sensitivities. *J. Atmos. Sci.,* **60,** 607–625.

Klein, S. A., and D. L. Hartmann, 1993: The seasonal cycle of low stratiform clouds. *J. Climate,* **6,** 1587–1606.

Kuang, Z., and C. S. Bretherton, 2006: A mass flux scheme view of a high-resolution simulation of transition from shallow to deep cumulus convection. *J. Atmos. Sci.,* **63,** 1895–1909.

Lock, A. P., A. R. Brown, M. R. Bush, G. M. Martin, and R. N. B. Smith, 2000: A new boundary layer mixing scheme. Part I: Scheme description and single-column model tests. *Mon. Wea. Rev.,* **128,** 3187–3199.

Neale, R., J. R. Richter, and M. Jochum, 2008: The impact of convection on ENSO: From a delayed oscillator to a series of events. *J. Climate,* **21,** 5904–5924.

Park, S., and C. B. Leovy, 2000: Winter North Atlantic low cloud anomalies associated with the Northern Hemispheric annular mode. *Geophys. Res. Lett.,* **27,** 3357–3360.

——, and ——, 2004: Marine low cloud anomalies associated with ENSO. *J. Climate,* **17,** 3448–3469.

Pincus, R., H. W. Barker, and J. J. Morcrette, 2003: A fast, flexible, approximate technique for computing radiative transfer in inhomogeneous cloud fields. *J. Geophys. Res.,* **108,** 4376, doi:10.1029/2002JD003322.

Rasch, P. J., and J. E. Kristjansson, 1998: A comparison of the CCM3 model climate using diagnosed and predicted condensate parameterizations. *J. Climate,* **11,** 1587–1614.

Richter, J. R., and P. J. Rasch, 2008: Effects of convective momentum transport on the atmospheric circulation in the Community Atmospheric Model, version 3. *J. Climate,* **21,** 1487–1499.

Siebesma, A. P., and Coauthors, 2003: A large eddy simulation intercomparison study of shallow cumulus convection. *J. Atmos. Sci.,* **60,** 1201–1219.

Uppala, S. M., and Coauthors, 2005: The ERA-40 Re-Analysis. *Quart. J. Roy. Meteor. Soc.,* **131,** 2961–3012.

von Salzen, K., and N. A. McFarlane, 2002: Parameterization of the bulk effects of lateral and cloud-top entrainment in transient shallow cumulus clouds. *J. Atmos. Sci.,* **59,** 1405–1430.

Wentz, F. J., 1997: A well-calibrated ocean algorithm for SSM/I. *J. Geophys. Res.,* **102,** 8703–8718.

Willmott, C. J., and K. Matsuura, 1995: Smart interpolation of annually averaged air temperature in the United States. *J. Appl. Meteor.,* **34,** 2577–2586.

Wood, R., and C. S. Bretherton, 2004: Boundary layer depth, entrainment, and decoupling in the cloud-capped subtropical and tropical marine boundary layer. *J. Climate,* **17,** 3575–3587.

Zhang, G. J., and N. A. McFarlane, 1995: Sensitivity of climate simulations to the parameterization of cumulus convection in the Canadian Climate Centre general circulation model. *Atmos.–Ocean,* **33,** 407–446.